Chemical Science

ROYAL SOCIETY OF CHEMISTRY

EDGE ARTICLE

View Article Online
View Journal | View Issue

Cite this: *Chem. Sci.*, 2022, **13**, 10281

All publication charges for this article have been paid for by the Royal Society of Chemistry

Received 20th June 2022
Accepted 22nd July 2022

DOI: 10.1039/d2sc03443c

rsc.li/chemical-science

Peptide-directed synthesis of chiral nano-bipyramids for controllable antibacterial application†

Panpan Chen,‡ Gaoyang Wang,‡ Changlong Hao, Wei Ma, Liguang Xu, Hua Kuang, Chuanlai Xu and Maozhong Sun *

The emergence of antibiotic resistance makes the therapeutic effect of traditional antibiotics far from satisfactory. Here, chiral gold nano-bipyramids (GBPs) with sea cucumber-like morphology are reported, and used in the fight against bacterial infection. Specifically, the dipeptide of D-/L-Cys-Phe (CF) caused the nano-bipyramids to form a spike shape with an optical anisotropy factor of 0.102 at 573 nm. The antibacterial effects showed that D-GBPs and L-GBPs could efficiently destroy bacteria with a death ratio of 98% and 70% *in vitro*. Also, both *in vivo* skin infection and sepsis models showed that the chiral GBPs could effectively promote wound healing and prevent sepsis in mice. Mechanistic studies showed that the binding affinity of D-GBPs ($1.071 \pm 0.023 \times 10^{8}$ M^{-1}) was 12.39-fold higher than L-GBPs ($8.664 \pm 0.251 \times 10^{6}$ M^{-1}) to protein A of *Staphylococcus aureus*, which caused further adsorption of D-GBPs onto the bacterial surface. Moreover, the physical destruction of the bacterial cell wall caused by the spike chiral GBPs, resulted in a stronger antibacterial effect for D-GBPs than L-GBPs. Furthermore, the excellent PTT of D-/L-GBPs further exacerbated the death of bacteria without any side-effect. Overall, chiral nano-bipyramids have opened a new avenue for improved antibacterial efficacy in the treatment of bacterial infections.

Introduction

Bacterial infection is one of the most serious threats to public health and although traditional antibiotic therapy is effective, drug-resistant bacteria[1,2] have become a serious global health problem due to the wide and excessive use of antibiotics. In particular, common microorganisms such as *Staphylococcus aureus*, *Klebsiella pneumoniae*, *Klebsiella pneumoniae*, *Acinetobacter baumannii*, *Pseudomonas aeruginosa* and *Enterobacter* can cause intractable nosocomial infection, leading to high levels of antibiotic resistance. When bacterial infection occurs in the body, the host immune system is activated to eliminate the invading bacteria, but uncontrolled and excessive inflammatory responses may lead to sepsis, multiple organ failure and even death.[3] Therefore, there is an urgent need to develop novel innovative technologies to combat bacterial infections.[4]

Antibacterial nanomaterials[5,6] are becoming effective alternative treatments against drug-resistant bacteria.[7,8] They have many excellent properties including adjustable physicochemical properties[9,10] (such as shape, particle size, and surface charge, composition) and their surfaces can be easily modified, which shows great potential for the treatment of diseases such as implantable bacterial infection.[11,12] Researchers have developed a series of antibacterial nanomaterials, such as nano enzymes,[13,14] silica nanoparticles, metals[15–18] and metal oxides.[19,20] The strong interaction between nanoparticles and the biological host is key to bacterial inhibition.[21] Through surface modification of nano materials, interaction with the biological interface can be produced.[22] Photothermal therapy (PTT) is a new and effective sterilization method[23,24] and during this process, the materials convert light energy into heat energy, which can effectively kill planktonic bacteria.[25,26] PTT irradiated by near infrared (NIR) light has been widely studied because it further improves its tissue penetration and remote-control ability.[27,28]

Recently, chiral nanomaterials have been developed extensively and by adjusting their optical properties, their chiral optical signal can be adjusted to the visible and near-infrared, which has been exploited in any fields.[29–31] Through the screening of chiral ligands, metal nano materials with different chiral structures can be constructed. For chiral ligands, the use of peptide sequences with a chiral conformation has become a means of controlling the growth and optical properties of nanomaterials.[32,33] At the same time, it also provides more ways

International Joint Research Laboratory for Biointerface and Biodetection, State Key Lab of Food Science and Technology, School of Food Science and Technology, Jiangnan University, Wuxi, Jiangsu, 214122, People's Republic of China. E-mail: smz@jiangnan.edu.cn

† Electronic supplementary information (ESI) available. See https://doi.org/10.1039/d2sc03443c

‡ The authors contributed equally to this paper.

and wider applications for the study of surface plasma properties.[34,35] Among noble metal nanomaterials, gold nanobipyramids (GNPs) represent a slender gold nanocrystal with an adjustable longitudinal plasma resonance wavelength (LSPR).[36] Due to its excellent photothermal conversion performance, good biocompatibility and photostability, GNPs have great potential for the treatment of bacterial infections.[37]

However, a single treatment does not provide a timely and effective antibacterial treatment. In order to promote precise effects, nano metal materials must be capable of intelligent function and morphologically designed,[38–40] such as hydrophilicity and targeted modification.[41] At the same time, they must overcome the disadvantages of poor targeting,[42–44] low permeability and weak diffusion in organisms, improve the biocompatibility and stability of materials,[45] and achieve efficient sterilization effects.[46] In addition, the special sharp structure of nanomaterials can cause physical damage to the bacterial cell wall and destroy it without any bacterial drug resistance effects.[47] Therefore, physical sterilization combined with photothermal effects could greatly improve their antibacterial efficacy.

In this work, we synthesized chiral GBPs with sea cucumber-like morphology through the modification of dipeptides. The biosafety and stability of the materials were improved by SH-PEG modification. The GBPs attached to bacteria at the infected site, played an effective antibacterial role with synergistic effects of PTT under NIR. It was found that D-type NPs induced a more robust antibacterial response than L-type NPs, due to the chirality-dependent difference in cell wall affinity. Moreover, its therapeutic effect in a mouse skin infection model and a sepsis model for the treatment of sepsis caused by *Staphylococcus aureus* was investigated.

Results and discussion

Characterization and photothermal properties of the D-/L-GBPs

Chiral GBPs were synthesized by the seed-mediated method (Fig. 1A).[48] Firstly, the biconical seeds (Au NBPs) with edge lengths of 60–240 nm were synthesized (Fig. 1B and S1†). Considering the size of Au NBPs spikes, we finally chose the Au NBPs of 100 nm as the seeds of subsequent experiments to further synthesize GBPs. Next, an aqueous growth solution containing $HAuCl_4$ (gold precursor), ascorbic acid (reducing agent) and chiral peptide Cys-Phe (CF) was prepared and then mixed with gold seeds. The ascorbic acid reduced Au^{3+} to Au^{+} to induce Au grow on the surface of the GNPs, resulting in chiral GBPs with a spike structure on their surfaces.

Then, the synthesis and quality of the chiral GBPs were confirmed by transmission electron microscopy (TEM), scanning electron microscopy (SEM), circular dichroism (CD) spectra, ultraviolet-visible absorption (UV-vis) spectra, X-ray diffraction (XRD), Infrared spectra (IR) and X-ray photoelectron spectra (XPS). TEM and SEM images revealed that the prepared D-/L-GBPs was approximately 200 ± 5.3 nm long and 50 ± 2.8 nm wide (Fig. 1C and D, S2†), and had good dispersion and uniformity. The CD spectrum of L-GBPs produced multiple

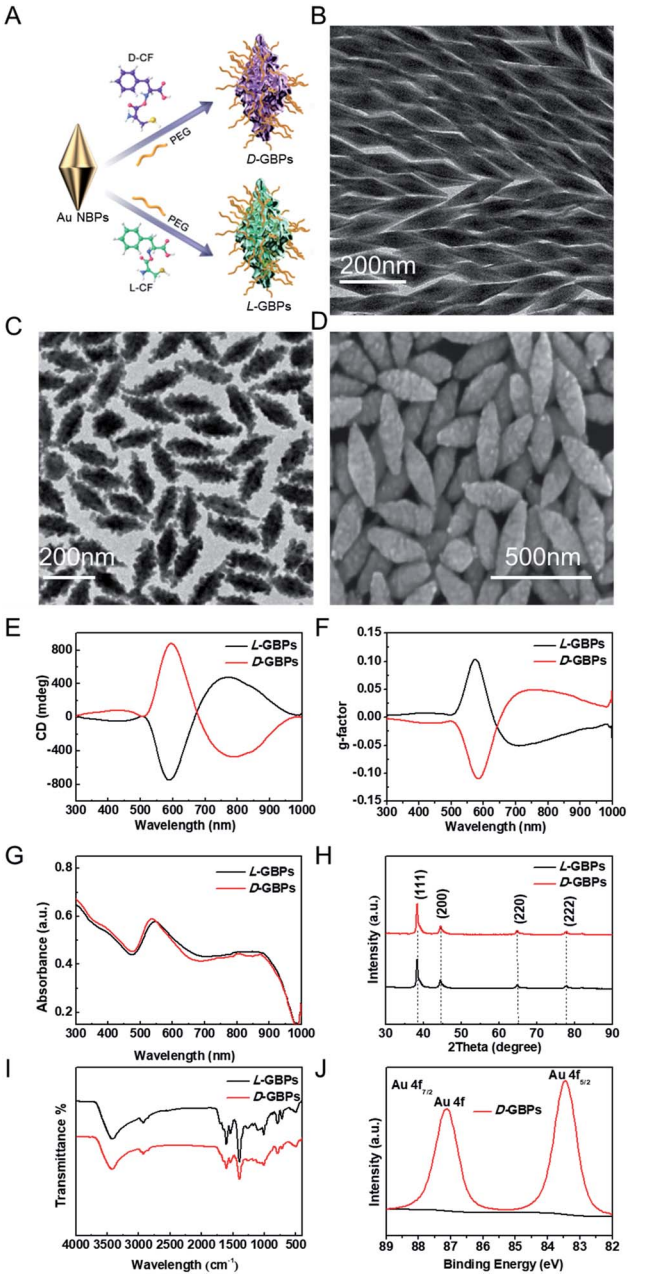

Fig. 1 Characterization and photothermal properties of the D-/L-GBPs. (A) Schematic diagram of D-/L-GBPs preparation. (B) TEM images of biconical seeds (Au NBPs). The (C) TEM and (D) SEM images of D-GBPs. The (E) CD, (F) *g*-factor and (G) UV-vis-NIR spectra of D-/L-GBPs. (H) XRD patterns, and (I) IR of D-/L-GBPs. (J) The XPS spectrum of D-GBPs.

CD bands at 505 nm (+), 573 nm (−) and 794 nm (+). The strongest chiral activity was at 573 nm (Fig. 1E). The CD spectra of D-GBPs and L-GBPs had mirror symmetry and showed that the maximum anisotropy factor (*g*-factor) was 0.102 at 573 nm (Fig. 1F). The LSPR of the GBPs showed a peak at 536 nm in the UV-Vis spectrum (Fig. 1G). XRD results confirmed a face centered cubic structure of gold atoms (Fig. 1H). The stretching vibration of –SH absorption peak at 2590 cm^{-1} in the infrared spectrum weakened its absorption after binding with the gold

seeds, which proved that the chiral dipeptide was successfully connected to the seeds (Fig. 1I). The XPS spectrum results are shown in Fig. 1J and S3† along with the high-resolution spectrum of the Au 4f orbit. Due to spin orbit coupling, the contour was displayed as bimodal. The value of 83.8 eV was regarded as a neat characteristic for the onset of Au^{+} with metallic-like properties. The chiral gold nano materials synthesized above had a stable structure, were well dispersed and a transparent homogeneous phase. The prepared samples showed no precipitation after long-term storage at room temperature. The photothermal properties of the materials was assessed by recording the temperature of the materials under near-infrared light irradiation (808 nm) through a thermal imager. It was observed that the temperature of the solution depends on its concentration, the duration of NIR exposure, and the light power. When a solution concentration of 55 μg mL^{-1} was exposed to NIR (0.8 W cm^{-2}) for 5 min, the solution temperature quickly reached over 45 °C (Fig. S4–S6†), while the temperature of the PBS solution without materials did not change significantly. When the GBPs concentration was consistent (55 μg mL^{-1}), the increase in the light power also lead to a sharp increase in the GBPs solution temperature. Excellent photothermal properties as well as good absorption of near-infrared light producing temperatures above body

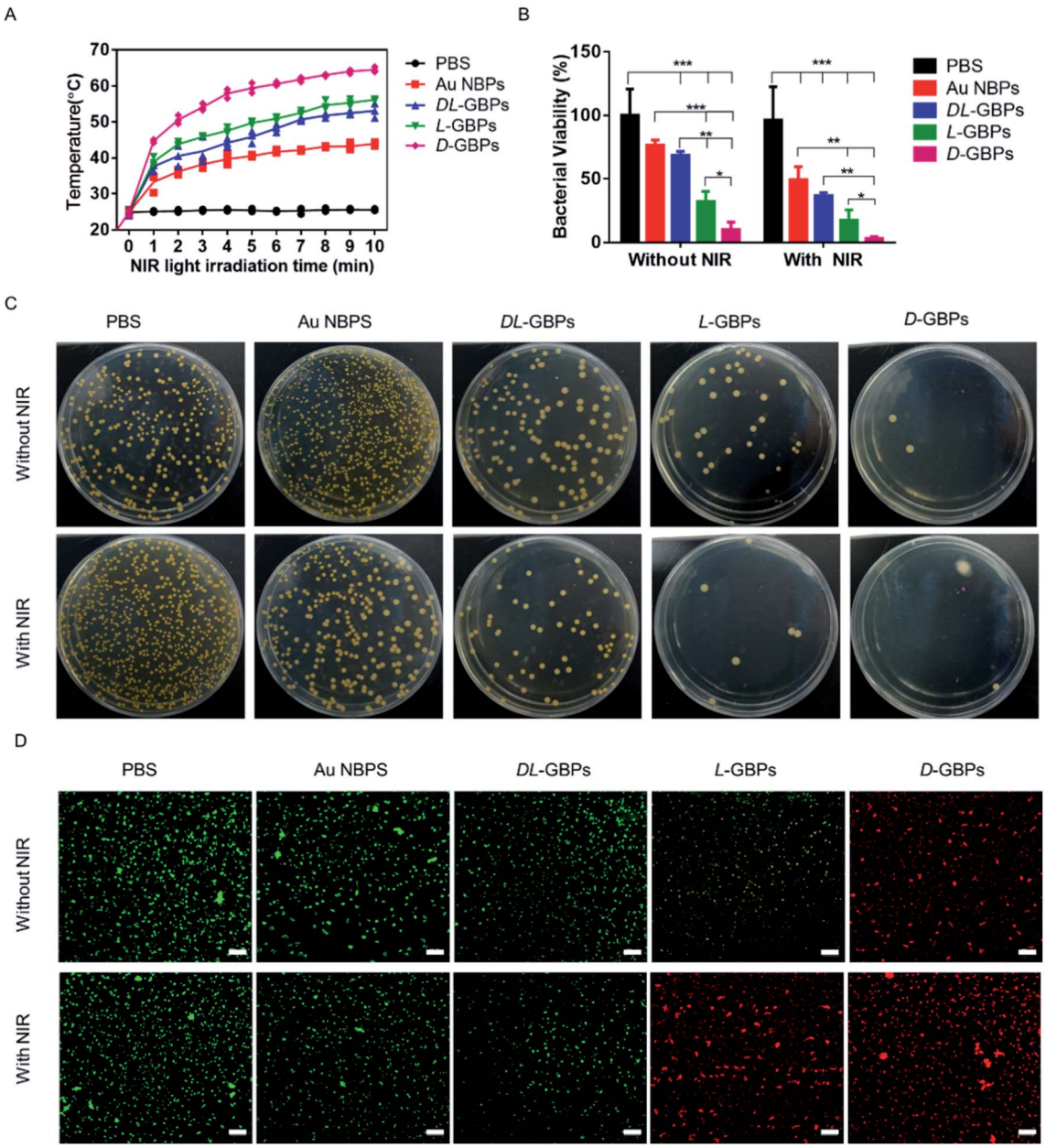

Fig. 2 Antibacterial activity of D-/L-GBPs *in vitro*. (A) Temperature changes of *Staphylococcus aureus* solution when the concentration of PBS, Au NBPs, DL-GBPs, D-GBPs and L-GBPs was 55 μg mL^{-1} under 808 nm laser irradiation, respectively. (B) Bacterial viability of *Staphylococcus aureus* after treated by different methods. $^{**}p < 0.01$. (C) Photographs of *Staphylococcus aureus* colonies after treated by different methods. (D) The Live/Dead assay of *Staphylococcus aureus* after processed by different methods (green: live, red: dead, scale: 20 μm).

temperature might lead to severe damage to the bacterial cell wall and therefore, GBPs have great potential for photothermal antibacterial therapy.

Next, the cell viability of primary uterine fibroblast (PCS-460-010) to D-/L-GBPs was determined using a 5-diphenyl-2-*H*-tetrazole bromide (MTT) assay to assess the phototoxicity and cytotoxicity of the materials. The cells were incubated with Au NBPs, DL-GBPs, L-GBPs or D-GBPs for 3 h at 37 °C, then irradiated with NIR (0–1.2 W cm^{-2}) for 10 min. It was found that the cell viability was higher than 90% of the control group, even when the light power reached 0.8 W cm^{-2} (Fig. S7†), suggesting that the photo-toxicity produced by the GBPs was weak and could be used as a candidate for PTT. Also, when the power was constant, cells incubated with different concentrations of materials and irradiated with NIR (0.8W cm^{-2}, 10 min) their activity remained high even if the concentration of the materials were up to 55 μg mL^{-1} (Fig. S7†), indicating that the sample had low cytotoxicity and maintained good biocompatibility during PTT. Therefore, in the following antibacterial experiments, we chose a low power intensity (808 nm, 0.8 W cm^{-2}) to eliminate adverse damage to the surrounding healthy tissues.

In vitro antibacterial activity of the D-/L-GBPs

Staphylococcus aureus was used as a model strain to study the antibacterial behavior of D-/L-GBPs. Au NBPs, DL-GBPs, L-GBPs and D-GBPs; these were incubated with bacteria under NIR (808 nm, 10 min) irradiation, and their temperature changes were recorded. It was found that the rise in temperature after treatment with D-/L-GBPs was more obvious than bacteria treated with Au NBPs, and the temperature with D-GBPs treatment was higher than seen with L-GBPs (Fig. 2A and S8†). Therefore, the results showed that D-/L-GBPs had significant antibacterial effects. Moreover, results were much more significant in the presence of NIR irradiation, which could reduce bacterial activity by 98 ± 1.5% (Fig. 2B) and the antibacterial activity after treatment with D-GBPs was significantly higher than that of L-GBPs. The antibacterial effect of DL-GBPs and Au NBPs was not as obvious however. In addition, standard plate counting results showed that D-GBPs under NIR irradiation was most effective at inhibiting *Staphylococcus aureus*, and almost no bacterial colonies were found in the plate, and this was consistent with the above results (Fig. 2C). The bacterial colonies treated with D-GBPs alone decreased by 79 ± 2.3%, indicating that D-/L-GBPs alone could not completely destroy the bacterial cells in this study. These results confirmed that D-/L-GBPs under NIR irradiation could strongly inhibit bacterial growth through the synergistic effect of PTT. To further evaluate the antibacterial effects, *in vitro* antibacterial activity was assessed using a Live/Dead two-color kit (Fig. 2D). Under the confocal fluorescence microscope, the live bacteria with intact cell membranes showed green fluorescence, and the dead bacteria with damaged cell membranes showed red fluorescence. When treated with PBS and Au NBPs alone, most bacteria survived (green), while treatment with D-/L-GBPs caused a certain number of bacteria to die, and a small number of bacteria were stained with red fluorescence. In contrast, the proportion of dead bacteria (red) increased significantly when treated with D-/L-GBPs under NIR irradiation, and the red increased significantly in the D-GBPs treated group. However, no significant increase in red fluorescence was observed in the PBS + NIR and Au NBPs + NIR treatment groups, indicating that they could not significantly increase their antibacterial effect through PTT and these findings are consistent with the results of plate counting. The above results showed that the synergistic antibacterial behavior of D-/L-GBPs can be used to treat implantable infectious bacteria effectively.

Antibacterial mechanism of D-/L-GBPs

The interaction between different configurations of chiral materials and bacteria was tested using fluorescence imaging (Fig. 3A). The Cy5.5-labeled chiral nanomaterial was used to investigate the interactions with bacterial walls. The experiment showed that when the materials were incubated with bacteria, the red fluorescence of D-GBPs overlapped well with the blue fluorescence of *Staphylococcus aureus* (Hoechst 33342), indicating that D-GBPs could adsorb onto the bacteria and penetrate their cell wall. At the same time, it was found that although the red fluorescence intensity of L-GBPs and DL-GBPs did not weaken, the fluorescence of their overlapping areas with Hoechst 33342 was relatively weak, most of them were free outside the bacteria or on its outer wall and could not penetrate the bacterial cell wall effectively. These results demonstrated that D-GBPs had stronger interaction with bacteria than L-GBPs and DL-GBPs, and it was easier to adsorb and penetrate bacterial cell wall. To further explore the reason for the different interactions between D-/L-GBPs and bacteria, we measured the affinity of D-/L-GBPs for protein A in the cell wall of *Staphylococcus aureus* by isothermal titration calorimetry (ITC) (Fig. 3B–D, S9†). The absolute K_a value for D-GBPs binding to protein A was $(1.071 \pm 0.023) \times 10^8\ M^{-1}$, the absolute K_a values of L-GBPs and DL-GBPs were $(8.664 \pm 0.251) \times 10^6\ M^{-1}$ and $(1.575 \pm 0.159) \times 10^6\ M^{-1}$, respectively. Therefore, the affinity of D-GBPs for protein A was 12.39-fold or 68-fold higher than L-GBPs or DL-GBPs. These data sufficiently explain the different adsorption capacity of the chiral configurations for the surface of *Staphylococcus aureus*. Therefore, a greater number of D-GBPs entered the bacteria, while L-GBPs and DL-GBPs were less adsorbed on the bacterial surface and most were unbound outside the bacteria due to their weaker affinity for protein A, which was consistent with our fluorescence results above. The difference in affinity made their numbers different when entering the bacteria, which further explains their difference in bacterial lethality. Next, the morphology of the bacteria was observed by SEM to further evaluate the antibacterial activity of D-/L-GBPs (Fig. 3E). The results showed that in the absence of NIR irradiation, the bacterial structures were damaged after treatment with the different materials, which might be due to the physical destruction of the bacterial cell wall caused by the sharp ends of the materials and the spike structure on their surfaces, resulting in the breakdown of the bacterial cell wall producing irregular holes. Among them, the structure of bacteria treated with D-GBPs appeared obviously damaged, which was consistent with

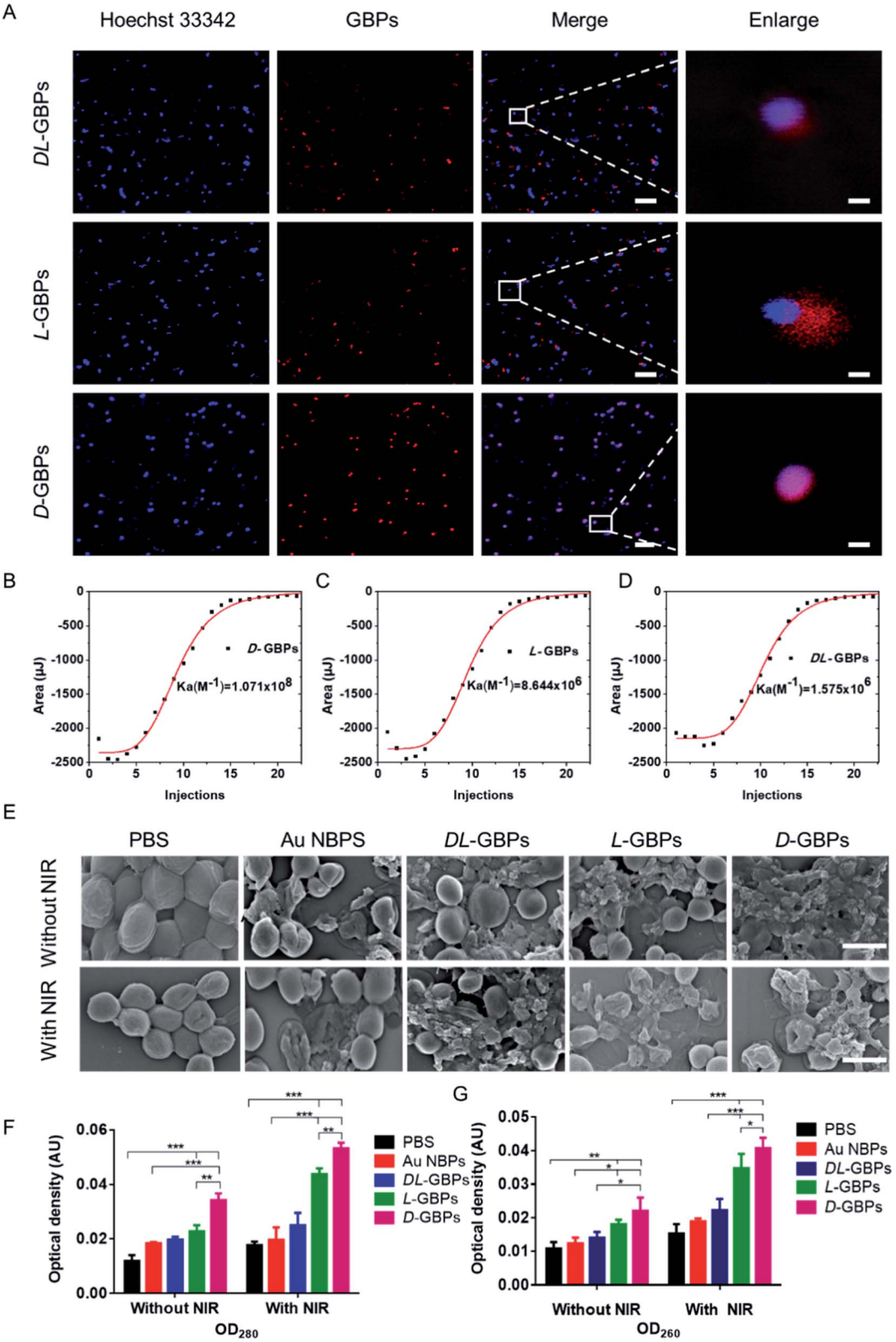

Fig. 3 Evaluation of antibacterial mechanism of D-/L-GBPs. (A) After material treatment, confocal fluorescence imaging was performed on *Staphylococcus aureus* and GBPs. The white dotted line part is the enlarged area of each bacterial image. Scale bar: 5 μm and 500 nm. The integrated heat data with respect to time for the titration of (B) D-GBPs, (C) L-GBPs and (D) DL-GBPs to protein A in the cell wall of *Staphylococcus aureus*. (E) SEM images of *Staphylococcus aureus* after various treatments. Scale bar: 1 μm. (F) The nucleic acid and (G) protein leakage of *Staphylococcus aureus* were treated by different methods by measuring the optical density. ***$p < 0.001$, **$p < 0.01$ and *$p < 0.05$.

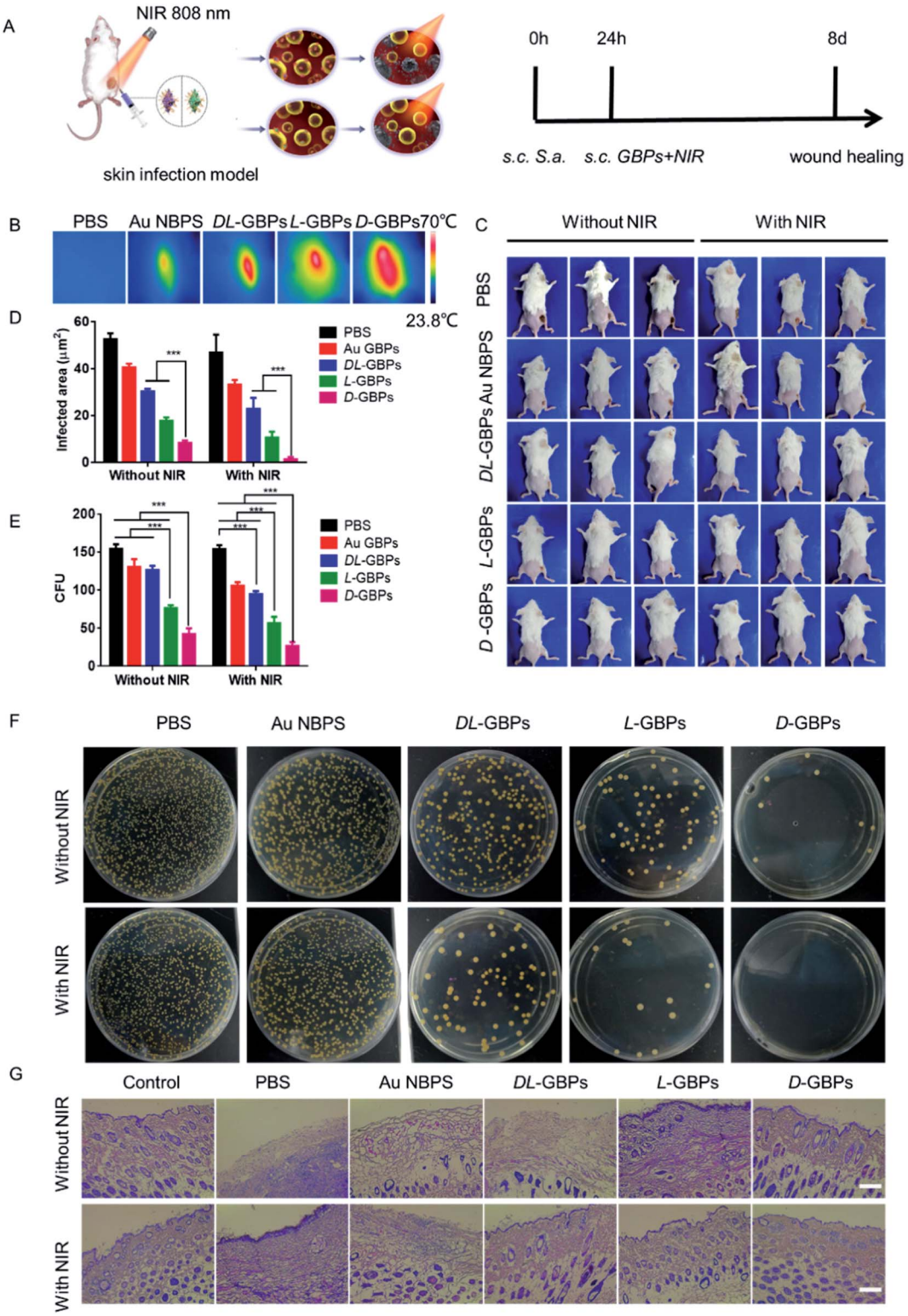

Fig. 4 Antibacterial activity of D-/L-GBPs *in vivo*. (A) Schematic diagram of mice skin infection model construction and treated with different materials. (B) Thermal imaging images of mice treated with D-/L-GBPs and PBS under NIR laser irradiation. (C) Photographs of *Staphylococcus aureus* infected mice treated with different materials. (D) Quantitative statistics of the skin infection area of mice treated with different materials. ***$p < 0.001$. (E) Quantitative statistics of the number of bacterial colonies determined by standard plate counting ($n = 3$). **$p < 0.01$, ***$p < 0.001$ and (F) photographs of bacterial colonies obtained from infected tissues of rats treated with different methods. (G) H & E staining of surrounding connective tissue after treatment with different methods on day 8 (scale: 20 μm).

our previous results showing that D-GBPs had higher penetrative efficiency for bacterial cell wall than L-GBPs and DL-GBPs. Moreover, the bacteria damage caused by the PTT effect of D-/L-GBPs further exacerbated the destruction of the bacterial cells and more bacteria lost their structural integrity under NIR irradiation. Furthermore, the degree of bacterial fragmentation was greatest in the NIR + D-GBPs treatment group. Whereas the bacteria in the control group (PBS) maintained normal shape with clear a boundary and the membrane integrity was intact with or without near-infrared light irradiation. We also measured the nucleic acid and protein leakage from *Staphylococcus aureus* (Fig. 3F and G) and the results showed that the nucleic acids and proteins in the cytoplasm and cell wall of the D-/L-GBPs treated bacteria were released into the surrounding milieu. Consistent with our previous results, the leakage of nucleic acids and protein from *Staphylococcus aureus* treated with NIR + D-GBPs increased significantly which further promote bacterial cell death and accelerate the destructive effect of GBPs on the bacteria.

Therefore, D-/L-GBPs was adsorbed onto the bacteria by their interaction with the bacterial cells, and D-GBPs showed higher penetrating efficiency for the bacterial cell wall when compared to L-GBPs due to its higher affinity for protein A, which destroyed the integrity of the bacterial cell structure and aggravated the mechanical deformation of the bacteria to a greater extent than L-GBPs. Furthermore, leakage of the bacterial contents was confirmed, causing further rupture and death of the bacteria. In addition, the PTT effect of D-/L-GBPs could further damage the bacteria under NIR irradiation. Through the above synergistic effect, it was found that *Staphylococcus aureus* was significantly inhibited by chiral materials.

In vivo antibacterial efficacy of D-/L-GBPs

After confirming an *in vitro* antibacterial role for D-/L-GBPs, two mouse infection models were applied to further evaluate the therapeutic effect of D-/L-GBPs *in vivo*. Here, mice were infected with 100 μL 10^6 CFU mL^{-1} *Staphylococcus aureus*, and then

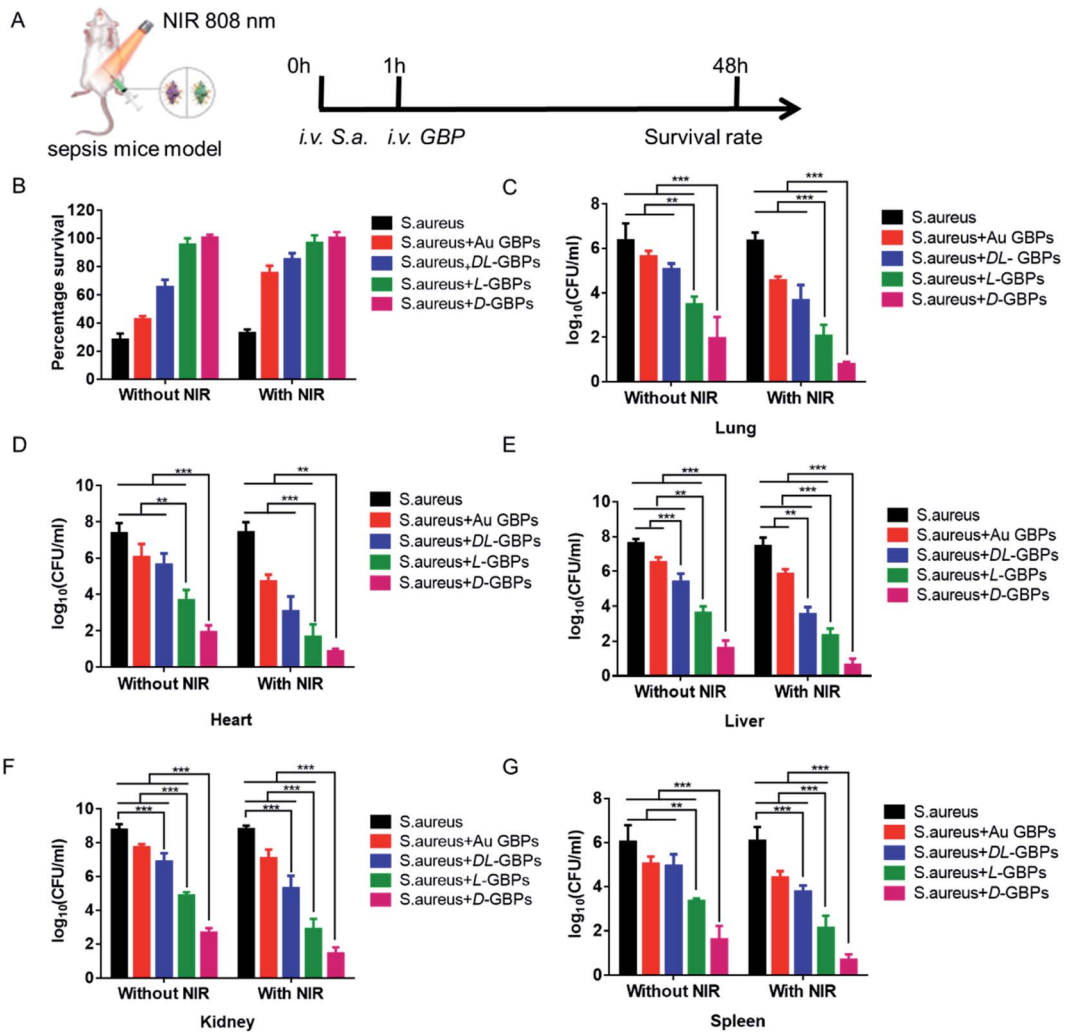

Fig. 5 Efficacy of D-/L-GBPs in septic mice model. (A) Experimental process of sepsis mice model construction and treated with different materials. (B) PBS, DL-GBPs, D-/L-GBPs and Au NBPs were used to treat the sepsis model. The number of bacteria in mice (C) lung, (D) heart, (E) liver, (F) kidney and (G) spleen after different treatment methods. $^{**}p < 0.01$, $^{***}p < 0.001$.

injected with 100 μL 55 μg mL^{-1} D-/L-GBPs solution and irradiated with NIR (0.8 W cm^{-2}) for 10 min (Fig. 4A). During this period, the change of temperature at the wound on the back of the mice was recorded using a thermal imager (Fig. 4B). The results showed that after 10 min of irradiation, the temperature of the infected area injected with D-/L-GBPs solution generally increased, and the temperature of the subcutaneous abscess in the D-GBPs treatment group was the highest, and reached as much as 60 °C ± 4.5, indicating that GBPs could effectively kill bacteria through photothermal effects. At the same time, it was observed that the temperature of surrounding normal tissues did not increase, indicating that the hyperthermia did not have any adverse effect on the normal tissues. This may be due to the strong interaction between D-/L-GBPs and bacteria, which lead to its specific adsorption. Next, the mouse wound was photographed, and the recovery of the wound was recorded. It was found that under NIR irradiation, no obvious inflammation was observed on the epidermis of the mice in the D-/L-GBPs treatment group on day 8. In particular, the wounds from the D-GBPs treatment group almost completely recovered, which was consistent with the state of the skin before infection (Fig. 4C and S10†), while the wound healing of the mice from the other groups was not obvious, and the abscesses and inflammation could still be observed. Our statistical analysis revealed that the wound area of the mice form the D-GBPs treatment group was much smaller than that seen in the other groups, and the wound area became smaller under NIR irradiation (Fig. 4D), demonstrating that D-/L-GBPs, in coordination with PTT, could significantly inhibit and kill bacteria *in vivo*. Next, we quantitatively evaluated *Staphylococcus aureus* in the skin abscess by standard plate counting methodology and it could be seen that the number of bacteria after NIR + D-/L-GBPs treatment was significantly reduced (Fig. 4E and F), which was consistent with the previous antibacterial effect *in vitro*. We then performed histological analysis of skin sections using hematoxylin and eosin (H & E) staining to examine the recovery of the infected skin tissue (Fig. 4G). In the group treated with PBS or NIR alone, signs of severe infected skin injury and inflammatory cell infiltration were observed. In contrast, the skin tissue inflammatory cell infiltration seen in the NIR + D-GBPs treated group decreased significantly, showing complete histological characteristics, indicating that this treatment had excellent therapeutic effect on skin infection.

Therefore, the antibacterial effect of D-/L-GBPs in a sepsis model was evaluated (Fig. 5A). Firstly, 100 μL 10^7 CFU mL^{-1} *Staphylococcus aureus* was injected intraperitoneally into mice leading to 90% mortality. Using statistical survival rates (Fig. 5B), it was found that the untreated infected mice died within 48 hours, while the mice injected with D-/L-GBPs were greatly protected, and the survival rate of mice was higher after NIR irradiation with mice from the D-GBPs + NIR group being in the best condition when compared to the other groups. Then, different organs derived from the infected mice were removed, and their respective bacterial contents were counted. The results showed that the number of bacteria in each organ (lung, heart, liver, kidney, spleen) decreased significantly after injection with D-/L-GBPs under NIR irradiation. Among them, the bacterial counts in mice treated with D-GBPs was the lowest and significantly lower than that of mice treated with L-GBPs (Fig. 5C–G). Compared with the *S. aureus* group, the number of white blood cells counted in mice treated by the different materials increased gradually, and the number of lymphocytes and neutrophils in blood gradually decreased (Fig. S11–S13†). The weight of the mice treated by the different materials gradually recovered (Fig. S14†). Among them, the recovery level in the D-GBPs + NIR group was the greatest. In addition, the typical pathological changes in each organ was also alleviated in the treatment group (Fig. S15†). These results revealed that D-/L-GBPs had significant antibacterial effect *in vivo* under NIR irradiation.

Conclusions

In summary, chiral gold nano materials (D-/L-GBPs) mediated by dipeptides were synthesized to resist bacterial infection. We found the chirality-dependent antibacterial effect that D-GBPs had much stronger at destroying bacteria than L-GBPs for *Staphylococcus aureus* both *in vitro* and *in vivo*. This study, therefore, provides a promising tool to further improve the therapeutic treatment of bacterial infection, including fatal bacterial infection, regulating systemic inflammatory responses and preventing multiple organ failure through chiral nanomaterials.

Data availability

The data supporting the findings of this study are available within the paper and its ESI.†

Author contributions

M. S., H. K. and C. X. conceived the project and designed the experiments. P. C. and G. W. were responsible for cell and animal experiments. W. M. and C. H. were responsible for spectroscopic measurements. C. X. and M. S. conceptualized the work. C. X. and H. K. supervised the study. P. C., G. W. and M. S. analysed the results and wrote the manuscript. X. L., H. K., C. X. and M. S. discussed the results and commented on the manuscript.

Conflicts of interest

There are no conflicts of interest to declare.

Acknowledgements

This work is financially supported by the National Science Foundation of China (21977038, 51902136).

References

1 S. Hussain, J. Joo, J. Kang, B. Kim, G. B. Braun, Z.-G. She, D. Kim, A. P. Mann, T. Mölder, T. Teesalu, S. Carnazza, S. Guglielmino, M. J. Sailor and E. Ruoslahti, Antibiotic-

loaded nanoparticles targeted to the site of infection enhance antibacterial efficacy, *Nat. Biomed. Eng.*, 2018, **2**(2), 95–103.

2 D. I. Andersson and D. Hughes, Antibiotic resistance and its cost: is it possible to reverse resistance?, *Nat. Rev. Microbiol.*, 2010, **8**(4), 260–271.

3 C. Y. Zhang, J. Gao and Z. Wang, Bioresponsive Nanoparticles Targeted to Infectious Microenvironments for Sepsis Management, *Adv. Mater.*, 2018, **30**(43), 1803618.

4 L. Feng, W. Shi, Q. Chen, H. Cheng, J. Bao, C. Jiang, W. Zhao and C. Zhao, Smart Asymmetric Hydrogel with Integrated Multi-Functions of NIR-Triggered Tunable Adhesion, Self-Deformation, and Bacterial Eradication, *Adv. Healthcare Mater.*, 2021, **10**(19), e2100784.

5 Q. Xin, Q. Liu, L. Geng, Q. Fang and J. R. Gong, Chiral Nanoparticle as a New Efficient Antimicrobial Nanoagent, *Adv. Healthcare Mater.*, 2017, **6**(4), 1601011.

6 M. Chen, J. Zhou, P. Ran, F. Lei, J. Meng, J. Wei and X. Li, Photoactivated Release of Nitric Oxide and Antimicrobial Peptide Derivatives for Synergistic Therapy of Bacterial Skin Abscesses, *Adv. Healthcare Mater.*, 2022, e2200199.

7 W. Wang, C. Hao, M. Sun, L. Xu, X. Wu, C. Xu and H. Kuang, Peptide Mediated Chiral Inorganic Nanomaterials for Combating Gram-Negative Bacteria, *Adv. Funct. Mater.*, 2018, **28**(44), 1805112.

8 L. Yuwen, Y. Sun, G. Tan, W. Xiu, Y. Zhang, L. Weng, Z. Teng and L. Wang, MoS_2@polydopamine-Ag nanosheets with enhanced antibacterial activity for effective treatment of Staphylococcus aureus biofilms and wound infection, *Nanoscale*, 2018, **10**(35), 16711–16720.

9 G. Wang, C. Hao, W. Ma, A. Qu, C. Chen, J. Xu, C. Xu, H. Kuang and L. Xu, Chiral Plasmonic Triangular Nanorings with SERS Activity for Ultrasensitive Detection of Amyloid Proteins in Alzheimer's Disease, *Adv. Mater.*, 2021, **33**(38), e2102337.

10 Z. Liang, C. Hao, C. Chen, W. Ma, M. Sun, L. Xu, C. Xu and H. Kuang, Ratiometric FRET Encoded Hierarchical ZrMOF @ Au Cluster for Ultrasensitive Quantifying MicroRNA In Vivo, *Adv. Mater.*, 2022, **34**(1), e2107449.

11 G. Fang, W. Li, X. Shen, J. M. Perez-Aguilar, Y. Chong, X. Gao, Z. Chai, C. Chen, C. Ge and R. Zhou, Differential Pd-nanocrystal facets demonstrate distinct antibacterial activity against Gram-positive and Gram-negative bacteria, *Nat. Commun.*, 2018, **9**(1), 129.

12 M. Sun, A. Qu, C. Hao, X. Wu, L. Xu, C. Xu and H. Kuang, Chiral Upconversion Heterodimers for Quantitative Analysis and Bioimaging of Antibiotic-Resistant Bacteria In Vivo, *Adv. Mater.*, 2018, **30**(50), e1804241.

13 F. Gao, T. Shao, Y. Yu, Y. Xiong and L. Yang, Surface-bound reactive oxygen species generating nanozymes for selective antibacterial action, *Nat. Commun.*, 2021, **12**(1), 745.

14 Z. Liu, S. Li, Z. Yin, Z. Zhu, L. Chen, W. Tan and Z. Chen, Stabilizing Enzymes in Plasmonic Silk Film for Synergistic Therapy of In Situ SERS Identified Bacteria, *Adv. Sci.*, 2022, **9**(6), e2104576.

15 C. Wang, Y. Wang, L. Zhang, R. J. Miron, J. Liang, M. Shi, W. Mo, S. Zheng, Y. Zhao and Y. Zhang, Pretreated Macrophage-Membrane-Coated Gold Nanocages for Precise Drug Delivery for Treatment of Bacterial Infections, *Adv. Mater.*, 2018, **30**(46), e1804023.

16 L. Wang, S. Li, J. Yin, J. Yang, Q. Li, W. Zheng, S. Liu and X. Jiang, The Density of Surface Coating Can Contribute to Different Antibacterial Activities of Gold Nanoparticles, *Nano Lett.*, 2020, **20**(7), 5036–5042.

17 L. M. Stabryla, K. A. Johnston, N. A. Diemler, V. S. Cooper, J. E. Millstone, S. J. Haig and L. M. Gilbertson, Role of bacterial motility in differential resistance mechanisms of silver nanoparticles and silver ions, *Nat. Nanotechnol.*, 2021, **16**(9), 996–1003.

18 Y. Jiang, W. Zheng, K. Tran, E. Kamilar, J. Bariwal, H. Ma and H. Liang, Hydrophilic nanoparticles that kill bacteria while sparing mammalian cells reveal the antibiotic role of nanostructures, *Nat. Commun.*, 2022, **13**(1), 197.

19 K. Zheng, K. Li, T. H. Chang, J. Xie and P. Y. Chen, Synergistic Antimicrobial Capability of Magnetically Oriented Graphene Oxide Conjugated with Gold Nanoclusters, *Adv. Funct. Mater.*, 2019, **29**(46), 1904603.

20 R. Wang, M. Shi, F. Xu, Y. Qiu, P. Zhang, K. Shen, Q. Zhao, J. Yu and Y. Zhang, Graphdiyne-modified TiO2 nanofibers with osteoinductive and enhanced photocatalytic antibacterial activities to prevent implant infection, *Nat. Commun.*, 2020, **11**(1), 4465.

21 D. P. Linklater, V. A. Baulin, X. Le Guevel, J. B. Fleury, E. Hanssen, T. H. P. Nguyen, S. Juodkazis, G. Bryant, R. J. Crawford, P. Stoodley and E. P. Ivanova, Antibacterial Action of Nanoparticles by Lethal Stretching of Bacterial Cell Membranes, *Adv. Mater.*, 2020, **32**(52), e2005679.

22 T. Zhao, L. Chen, P. Wang, B. Li, R. Lin, A. Abdulkareem Al-Khalaf, W. N. Hozzein, F. Zhang, X. Li and D. Zhao, Surface-kinetics mediated mesoporous multipods for enhanced bacterial adhesion and inhibition, *Nat. Commun.*, 2019, **10**(1), 4387.

23 J. Li, X. Liu, L. Tan, Z. Cui, X. Yang, Y. Liang, Z. Li, S. Zhu, Y. Zheng, K. W. K. Yeung, X. Wang and S. Wu, Zinc-doped Prussian blue enhances photothermal clearance of Staphylococcus aureus and promotes tissue repair in infected wounds, *Nat. Commun.*, 2019, **10**(1), 4490.

24 J. Zeng, Y. Wang, Z. Sun, H. Chang, M. Cao, J. Zhao, K. Lin and Y. Xie, A novel biocompatible PDA/IR820/DAP coating for antibiotic/photodynamic/photothermal triple therapy to inhibit and eliminate *Staphylococcus aureus* biofilm, *Chem. Eng. J.*, 2020, **394**, 125017.

25 D. Zhang, X. Qin, T. Wu, Q. Qiao, Q. Song and Z. Zhang, Extracellular vesicles based self-grown gold nanopopcorn for combinatorial chemo-photothermal therapy, *Biomaterials*, 2019, **197**, 220–228.

26 G. B. Hwang, H. Huang, G. Wu, J. Shin, A. Kafizas, K. Karu, H. D. Toit, A. M. Alotaibi, L. Mohammad-Hadi, E. Allan, A. J. MacRobert, A. Gavriilidis and I. P. Parkin, Photobactericidal activity activated by thiolated gold nanoclusters at low flux levels of white light, *Nat. Commun.*, 2020, **11**(1), 1207.

27 L. Zhang, Y. Wang, J. Wang, Y. Wang, A. Chen, C. Wang, W. Mo, Y. Li, Q. Yuan and Y. Zhang, Photon-Responsive

Antibacterial Nanoplatform for Synergistic Photothermal-/Pharmaco-Therapy of Skin Infection, *ACS Appl. Mater. Interfaces*, 2019, **11**(1), 300–310.

28 L. X. Yan, L. J. Chen, X. Zhao and X. P. Yan, pH Switchable Nanoplatform for In Vivo Persistent Luminescence Imaging and Precise Photothermal Therapy of Bacterial Infection, *Adv. Funct. Mater.*, 2020, **30**(14), 1909042.

29 Y. Zhang, Z.-b. Qu, C. Jiang, Y. Liu, R. Pradeep Narayanan, D. Williams, X. Zuo, L. Wang, H. Yan, H. Liu and C. Fan, Prescribing Silver Chirality with DNA Origami, *J. Am. Chem. Soc.*, 2021, **143**(23), 8639–8646.

30 E. Longo, A. Orlandin, F. Mancin, P. Scrimin and A. Moretto, Reversible Chirality Control in Peptide-Functionalized Gold Nanoparticles, *ACS Nano*, 2013, **7**(11), 9933–9939.

31 M. Caricato, A. K. Sharma, C. Coluccini and D. Pasini, Nanostructuring with chirality: binaphthyl-based synthons for the production of functional oriented nanomaterials, *Nanoscale*, 2014, **6**(13), 7165–7174.

32 H.-E. Lee, H.-Y. Ahn, J. Mun, Y. Y. Lee, M. Kim, N. H. Cho, K. Chang, W. S. Kim, J. Rho and K. T. Nam, Amino-acid- and peptide-directed synthesis of chiral plasmonic gold nanoparticles, *Nature*, 2018, **556**(7701), 360–365.

33 J. M. Slocik, A. O. Govorov and R. R. Naik, Plasmonic Circular Dichroism of Peptide-Functionalized Gold Nanoparticles, *Nano Lett.*, 2011, **11**(2), 701–705.

34 M. Caricato, N. J. Leza, K. Roy, D. Dondi, G. Gattuso, L. S. Shimizu, D. A. Vander Griend and D. Pasini, A Chiroptical Probe for Sensing Metal Ions in Water, *Eur. J. Org. Chem.*, 2013, **2013**(27), 6078–6083.

35 M. Agnes, A. Arabi, M. Caricato, A. Nitti, D. Dondi, K. Yannakopoulou, M. Patrini and D. Pasini, Helical Nanofibers Formed by Palladium-Mediated Assembly of Organic Homochiral Macrocycles Containing Binaphthyl and Pyridyl Units, *ChemPlusChem*, 2021, **86**(2), 270–274.

36 J. H. Lee, K. J. Gibson, G. Chen and Y. Weizmann, Bipyramid-templated synthesis of monodisperse anisotropic gold nanocrystals, *Nat. Commun.*, 2015, **6**, 7571.

37 M. Zhang, H. Zhang, J. Feng, Y. Zhou and B. Wang, Synergistic chemotherapy, physiotherapy and photothermal therapy against bacterial and biofilms infections through construction of chiral glutamic acid functionalized gold nanobipyramids, *Chem. Eng. J.*, 2020, **393**, 124778.

38 H. Koide, A. Okishima, Y. Hoshino, Y. Kamon, K. Yoshimatsu, K. Saito, I. Yamauchi, S. Ariizumi, Y. Zhou, T. H. Xiao, K. Goda, N. Oku, T. Asai and K. J. Shea, Synthetic hydrogel nanoparticles for sepsis therapy, *Nat. Commun.*, 2021, **12**(1), 5552.

39 S. Tian, H. Bai, S. Li, Y. Xiao, X. Cui, X. Li, J. Tan, Z. Huang, D. Shen, W. Liu, P. Wang, B. Z. Tang and C. S. Lee, Water-Soluble Organic Nanoparticles with Programable Intermolecular Charge Transfer for NIR-II Photothermal Anti-Bacterial Therapy, *Angew. Chem., Int. Ed. Engl.*, 2021, **60**(21), 11758–11762.

40 X. Wu, M. Yang, J. S. Kim, R. Wang, G. Kim, J. Ha, H. Kim, Y. Cho, K. T. Nam and J. Yoon, Reactivity Differences Enable ROS for Selective Ablation of Bacteria, *Angew. Chem., Int. Ed. Engl.*, 2022, e202200808.

41 N. M. O. Andoy, K. Jeon, C. T. Kreis and R. M. A. Sullan, Multifunctional and Stimuli-Responsive Polydopamine Nanoparticle-Based Platform for Targeted Antimicrobial Applications, *Adv. Funct. Mater.*, 2020, **30**(40), 2004503.

42 B. Peng, X. Zhang, D. Aarts and R. P. A. Dullens, Superparamagnetic nickel colloidal nanocrystal clusters with antibacterial activity and bacteria binding ability, *Nat. Nanotechnol.*, 2018, **13**(6), 478–482.

43 X. Hou, X. Zhang, W. Zhao, C. Zeng, B. Deng, D. W. McComb, S. Du, C. Zhang, W. Li and Y. Dong, Vitamin lipid nanoparticles enable adoptive macrophage transfer for the treatment of multidrug-resistant bacterial sepsis, *Nat. Nanotechnol.*, 2020, **15**(1), 41–46.

44 H. Wang, M. Wang, X. Xu, P. Gao, Z. Xu, Q. Zhang, H. Li, A. Yan, R. Y. Kao and H. Sun, Multi-target mode of action of silver against Staphylococcus aureus endows it with capability to combat antibiotic resistance, *Nat. Commun.*, 2021, **12**(1), 3331.

45 Y. Long, L. Li, T. Xu, X. Wu, Y. Gao, J. Huang, C. He, T. Ma, L. Ma, C. Cheng and C. Zhao, Hedgehog artificial macrophage with atomic-catalytic centers to combat Drug-resistant bacteria, *Nat. Commun.*, 2021, **12**(1), 6143.

46 Y. Qiao, X. Liu, B. Li, Y. Han, Y. Zheng, K. W. K. Yeung, C. Li, Z. Cui, Y. Liang, Z. Li, S. Zhu, X. Wang and S. Wu, Treatment of MRSA-infected osteomyelitis using bacterial capturing, magnetically targeted composites with microwave-assisted bacterial killing, *Nat. Commun.*, 2020, **11**(1), 4446.

47 X. Wu, L. Mu, M. Chen, S. Liang, Y. Wang, G. She and W. Shi, Bifunctional Gold Nanobipyramids for Photothermal Therapy and Temperature Monitoring, *ACS Appl. Bio Mater.*, 2019, **2**(6), 2668–2675.

48 A. Sánchez-Iglesias, N. Winckelmans, T. Altantzis, S. Bals, M. Grzelczak and L. M. Liz-Marzán, High-Yield Seeded Growth of Monodisperse Pentatwinned Gold Nanoparticles through Thermally Induced Seed Twinning, *J. Am. Chem. Soc.*, 2017, **139**(1), 107–110.